2010 IEEE International Conference on Robotics and Automation
Anchorage Convention District
May 3-8, 2010, Anchorage, Alaska, USA

DSAC – Dynamic, Single Actuated Climber: Local Stability and Bifurcations

Amir Degani, Howie Choset, and Matthew T. Mason

Abstract— **This paper investigates a novel mechanism, called DSAC for Dynamic, Single Actuated Climber, which propels itself upwards by oscillating its leg in a symmetric fashion using a single actuator. This mechanism achieves dynamic, vertical motion while retaining simplicity in design and control.**

We explore the local orbital stability of the DSAC mechanism. We use the Poincaré map method with a well chosen Poincaré section to simplify the problem by reducing the dimension of the Poincaré map to 3-dimensions. We find the stable regions while varying the controls input and some of the mechanism's parameters. Moreover, in response to a continuous change in a parameter of the mechanism, the symmetric and steady stable gait of the mechanism gradually evolves through a regime of period doubling bifurcations.

I. INTRODUCTION

Humans and even more so animals use dynamic motions in everyday tasks such as running, jumping over obstacles, throwing objects, and climbing. Other than speed, why are dynamic motions superior to slower, quasistatic motions? There are two main reasons. First, to overcome the obstacles that defeat quasistatic machines. As an example, a human rock climber can reach a distant handholds if he leaps upward. Second, in an articulated, engineered, mechanism, the use of dynamic motions might enable simpler design. The use of dynamic movements can reduce the number of necessary active degrees of freedom – a minimalist mechanism. In the context of this work, the minimalist approach is the attempt to find the simplest mechanism that is capable of performing a given task. Simplicity of a system can be defined in different ways. In general one tries to minimize the amount of sensory input, actuation or computation.

Although dynamic motions can be superior to the quasistatic ones, dynamic mechanisms are rare. The reason lies in the complexity of the design. In order to make such a mechanism locomote robustly, it should be designed carefully with high accuracy to reduce uncertainty while moving dynamically and with high powered motors to achieve these dynamic motions. Most importantly these dynamic machines should be controlled at high speeds since the movements are fast. These reasons deter most designers from entering into this realm. In this paper a new mechanism is proposed that achieves these dynamic motions with an extremely simple mechanism. This minimalist mechanism – DSAC, for Dynamic Single Actuated Climber comprises a single actuated joint connecting two links. By using dynamic motions this mechanism is able to climb up a chute between two parallel walls. The goal of this paper is to show how dynamic motions can help design a minimalist mechanism and explore this novel, single actuated mechanism which is able to climb vertically between two parallel walls. We believe this mechanism is a good platform to demonstrate how dynamic motions do not inherently imply mechanical complexity, nor do they imply complex control. This paper extends the the work in [8], were we introduced a handful of assumptions and simplification that enabled us to obtain closed form approximations of the robot motion. Although this method did enable closed form solutions, it caused the analysis to lose its generality. In the current paper we depart from most of these simplifications and assumptions in order to generalize the analysis to a larger range of mechanisms and initial conditions. Indeed, using the current non-linear analysis we have found interesting phenomena including period-doubling bifurcations. For a detailed description of the analysis done here we refer the reader to [7].

This work has been supported in part by NSF Grant IIS 08030826 and by the Defense Advanced Research Projects Agency. This work does not necessarily reflect the position or the policy of the Government. No official endorsement should be inferred.

A. Degani, H. Choset and M. Mason are with the Robotics Institute, Carnegie Mellon University, 5000 Forbes Avenue, Pittsburgh, PA, USA <adegani,choset,mason>@cs.cmu.edu

II. RELATED WORK

A. Minimalism

Previous minimalism works have dealt with manipulation tasks such as in [4], [9], [13] and locomotion, such as the Acrobot [2] and the passive dynamic walkers described below [14], [10].

The mechanism described in this work extends the minimalism in locomotion from horizontal motions to vertical, climbing motions. The mechanism is able to achieve a climbing task, albeit a simple one, without sensing and control, with a symmetrically oscillating single actuator and a simple mechanical design.

B. Passive dynamic walking robots

McGeer, who initiated the work on passive dynamic walking [14] showed that a properly designed walking machine can walk down a gentle slope without any active control or energy input, other than potential energy from the slope. The mass and link length parameters can be chosen so that the natural dynamics of the walker enters a stable limit cycle from a basin-of-attraction of initial conditions. This principle has been used in the design of passive walkers with counter-swinging arms [6]. We use a similar tactic in our mechanism but instead of using gravity as a "dumb" actuator, we use a fixed symmetric oscillation.

C. Climbing robots

One aspect of the current work that differs from the work described above is that locomotion occurs largely in the vertical direction. While a number of wheeled robots have been designed for locomotion in vertical pipes, our work is more closely related to articulated (e.g., legged) climbing robots. Most such robots are quasistatic (e.g., [1], [3], [12]).

Unlike the quasistatic climber, only a few mechanisms have been proposed to achieve a vertical climbing task using dynamic motions. Clark et al. [5] analyzed and designed a cockroach inspired dynamic climbing robot which resembles a biologically based template for dynamic vertical climbing. Their robot comprises a main rigid body with two linearly moving hands with springs. Two main differences sets the DSAC apart from their dynamic climber. First, their mechanism is more complex in design since it uses two motors, energy storing springs, and a crank mechanism. Second, its climbing motion is similar to brachiating, flightless motion. During all times one arm is fixed to the ground. Lastly, in contrast to the DSAC mechanism, the cockroach inspired robot does not use reaction forces from walls but rather uses spines to attach itself to a carpet covered wall.

III. MODELING

In simulations and experiments this system exhibits stable periodic climbing motions. The goal of our analysis is to produce a model that exhibits behavior similar to that of the experiments and simulations. The DSAC mechanism is planar and consists of two links; the first is the leg which contacts the wall only at its distal tip. The second link is the main body which is connected to the leg through an actuated revolute joint (Fig. 1). The leg has mass M, moment of inertia J_L and length L. Its center of mass is located at actuated joint. The body is assumed to be thin with a point mass m concentrated at the end of the body, moment of inertia $J_l = 0$, and total length l. The body does not collide with the leg nor with the walls. The cartesian coordinates (x,y) are chosen at the distal end of the leg, the angle of the leg relative to the vertical is θ, and the angle between the two links is ϕ. The motion between the two links is set to be a sinusoid $\phi(t) = A\sin(\omega t)$, where A and ω are the amplitude and angular frequency of the sinusoid, respectively. For simplicity, the inertial frame is chosen on the symmetric line half of the distance between the two parallel walls.

To analyze the behavior of the mechanism, the motion is split into three phases: flight, impact, and stance phase. By using the final state of one phase as the initial values of the next phase we can analyze and simulate the whole climbing motion. Since the environment is symmetric (two parallel walls), we can include a "flip" of coordinates during impact phase, this will enable the equations to always represent a robot leaping from the right towards the left wall.

A projection of the phase plot onto the θ, $\dot{\theta}$ plane of a climbing gait from one wall to the other including the "flip" is depicted in Fig. 2. This phase plot portrays the important information of the climbing cycle. In fact, we will later

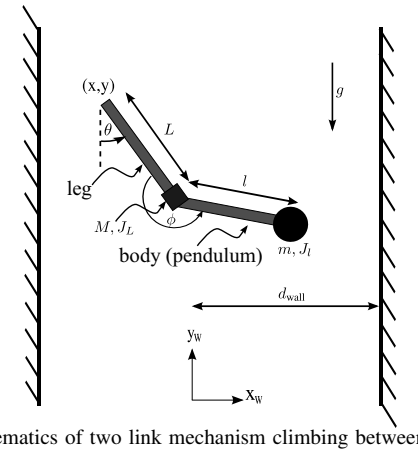

Fig. 1. Schematics of two link mechanism climbing between two parallel walls.

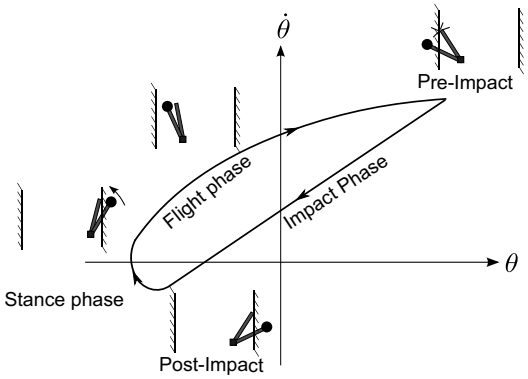

Fig. 2. Projection of phase plot onto the θ, $\dot{\theta}$ plane of a typical climbing motion including a "flip" at impact. Cartoon figures of each phase are also depicted.

show that these two state variables together with a variable corresponding to phase between the two links are all the information needed to portray the motion of the mechanism.

A few hypotheses and assumptions are used throughout in order to simplify the analysis. We assume that the impact model is instantaneous and inelastic, where no slipping or rebound occurs. The external forces during the impact can be represented by impulses, which may result in an instantaneous change in the velocities but not in the configuration. Since the actuator has a known sinusoidal trajectory, during the impact the motor can apply a high torque to keep itself on track. Moreover, the angular momentum around the contact point is constant hence the angular velocity of the leg can be calculated.

During the stance phase the leg is in contact with the wall. Due to high friction between the leg and the wall, no sliding will occur and the contact point is treated as a frictionless pin joint. We only consider the gait where the distal end of the leg hits the wall. We derived the equations of motion in Mathematica$^{\text{TM}}$, while numerical calculations were done in Matlab$^{\text{TM}}$.

Since the angle between the two links, ϕ, is sinusoidal, it will not be part of the state of the robot. This forced periodic input turns the equations of motion into a non-autonomous system. Such periodic forced system can then be converted

into an autonomous system as shown in [11]. The state of the system z is $(q,\dot{q})$, where $q=(x,y,\theta,\tau)\in\mathbb{R}^2\times\mathbb{S}^1\times\mathbb{S}^1$, $\tau=\omega t \pmod{2\pi}\in\mathbb{S}^1$, and $\dot{q}=(\dot{x},\dot{y},\dot{\theta},\omega)$. The addition of τ and ω comes from the conversion to an autonomous system.

We use nondimensional parameters in our equations of motion. We omit the derivation of the nondimensional equations are motion due to space limitation. See [7] for detailed derivation.

IV. ANALYSIS

A. Poincaré map and corresponding Poincaré section

As mentioned previously, our system exhibits periodic motions due to the forced periodic constraint ($\phi(t)$). Moreover, the system is a *hybrid* system, one that cannot be described as a single continuous flow but only as a collection of continuous flows with discrete changes during the transitions. In our system, these discrete changes occur while impacting the walls. Due to these facts, a useful tool to analyze stability is the Poincaré map [11]. This tool converts the study of the hybrid periodic flow of our mechanism into a nonlinear discrete mapping on a lower dimensional space. By looking at the crossing of the flow with a hyperplane one can now analyze this discrete system instead of the more complicated hybrid flow. Period-1 motion, i.e., climbing motion which returns to its initial state after one period, will correspond to a single fixed point on the Poincaré section. Period-k motion, i.e., flow that returns to the same state after k periods, will correspond to k points on this section. The Poincaré map defined in this work maps one state of the climbing robot, just after leaving the wall, to the state where the robot leaves the next wall. This is done by solving the equations of motion of the flight, impact, and stance phases numerically.

We can define the Poincaré map from the Poincaré section mapped back to this section by $\mathbf{P}$

$$z_{k+1}=\mathbf{P}(z_k), \tag{1}$$

where $\mathbf{P}$ is the map, z_k and z_{k+1} are states in the reduced spaces on the Poincaré section before and after the map, respectively. The dimension of reduced space on the Poincaré section can be extremely small if the section is chosen wisely. For this system, a convenient section to choose as the Poincaré section is the instant of release from the wall, i.e., the transition from stance to flight phase. This occurs when the normal contact force λ_n passes through zero from negative to positive. Because during stance phase the end of the leg is touching the wall ($x=d_{wall}$), no rebound ($\dot{x}=0$) or slippage ($\dot{y}=0$) occurs , we can define a reduced dimensional hyperplane Σ as the Poincaré section

$$\begin{aligned}\Sigma=\{&(x,\theta,\dot{x},\dot{y},\dot{\theta},\tau)\in\mathbb{R}^4\times\mathbb{S}^1\times\mathbb{S}^1\\ &\mid x=d_{wall},\dot{x}=0,\dot{y}=0,\lambda_n(z,\tau)=0\}\end{aligned} \tag{2}$$

If the mechanism reaches the wall during the climbing cycle, then the state z must lie on Σ. Other motions which do not reach the wall cannot be analyzed using this method, however, they are not of interest since pushing off the wall is needed for stable climbing.

Although the Poincaré section reduces the state tremendously (from eight to three), it is not trivial to calculate the exact transition since the contact forces need to be calculated. In this paper we simplify the section even further by assuming that the transition between stance and flight phases occurs when the acceleration of the swinging leg (ϕ) changes sign, i.e., when $\ddot{\phi}=-A\omega^2\sin(\omega t)=0$. This event occurs when $\tau=\omega t \pmod{2\pi}=2\pi$. This assumption is nearly correct in most climbing scenarios. The new Poincaré section can therefore be defined as

$$\begin{aligned}\Sigma=\{&(x,\theta,\dot{x},\dot{y},\dot{\theta},\tau)\in\mathbb{R}^4\times\mathbb{S}^1\times\mathbb{S}^1\\ &\mid x=d_{wall},\dot{x}=0,\dot{y}=0,\tau=2\pi\}\end{aligned} \tag{3}$$

In this Poincaré section all state variables are constrained, except θ and $\dot{\theta}$. Therefore, the Poincaré map is defined as

$$\mathbf{P}:\mathbb{S}^1\times\mathbb{R}\to\mathbb{S}^1\times\mathbb{R},$$

including only $\theta,\dot{\theta}$.

B. Local stability

We refer to stability of the climbing mechanism as the local orbital stability, i.e., the stability of an orbit in phase space around a fixed point. In order to find this kind of stability we must first find the fixed point of the Poincaré map, then linearize the Poincaré map around the fixed point, and finally find the eigenvalues of this linearized Poincaré map (Jacobian). For an orbitally stable cycle, the eigenvalues lie within the unit circle; i.e., their moduli are strictly less than one. This investigation is conducted numerically by first using the Newton-Raphson method to find the fixed point, and then calculating the Jacobian (linearized Poincaré map) and its eigenvalues numerically.

1) Fixed point search: The fixed point is the initial state of the mechanism that will map back to itself after one Poincaré map. Thus, we need to solve the equation

$$\mathbf{F}(z)\triangleq z-\mathbf{P}(z)=0. \tag{4}$$

This search is done by fixing the mechanism parameters and using the multidimensional Newton-Raphson method to search for the state that will map back to itself. The solution is not guaranteed and may not be unique. Note that during the Newton-Raphson search we need to solve the Poincaré map, i.e., forward simulate the three phases. During the flight phase, if the mechanism does not reach the wall after a certain integration time it is concluded that there is no fixed point. In fact, even if there is a fixed point, it will not be of interest for our climbing analysis because it will likely not be climbing at all.

2) Linearized Poincaré map and eigenvalues: The linearized Poincaré map around the fixed point which was previously found, is the Jacobian of the map. Calculating the Jacobian is done numerically using the forward difference approximation. Finally we numerically calculate the eigenvalues of the Jacobian and check to see if they all lie inside the unit circle. If so the motion is orbitally stable around this fixed point.

TABLE I

NONDIMENSIONAL PARAMETERS FOR RESULTS SECTION.

Parameter	Description	Value
m_s	Mass ratio $\frac{m}{m+M}$	0.7
l_s	Link length ratio $\frac{l}{L}$	$0.8^{\dagger}$
L_s	Link to walls gap ratio $\frac{L}{d_{wall}}$	$1\frac{2}{3}$
J_{Ls}	Nondimensional inertia $\frac{J_L}{L^2(m+M)}$	0.00355
γ	Nondimensional gravity $\frac{g}{d_{wall}\omega^2}$	$0.03486^{\dagger}$
A	Amplitude	$0.8^{\dagger}$
Parameters marked with † are varied in the current analysis		

V. ANALYSIS RESULTS

Using the analysis process described earlier we explore the orbital stability characteristics of a typical DSAC mechanism. The results given here are proof-of-concept examples of interesting phenomena and are not comprehensive. The results shown here are for the mechanism and environment parameters given in Table I[1]. Notice that the effective gravity is a tenth of the normal gravity. This will later help us in the experimental section to obtain interesting climbing phenomena using slower motor speeds.

A. Varying frequency and amplitude

Figure 3 shows the stability plot of the specific mechanism with parameters from Table I while varying ω and A. This plot is obtained by finding fixed points, linearizing around them and using the eigenvalues of the Jacobian to check if a stable orbit exists. This plot reveals three important regions. The first is the region where no fixed point was found (Fig. 3- bottom left region). This does not mean that there is necessarily no fixed point, just that the integration was stopped after a certain amount of time during which the mechanism did not reach the opposite wall. The central region is the period-1 stable region. This area is where the climbing gait is a symmetric, stable period-1. The third region depicts the period-1 non-stable together with the period-2 stable (Fig. 3- top right region). The fixed point search found two fixed points, one that maps back to itself (period-1) and another that maps back to itself only after two cycles (period-2). The eigenvalues of the Jacobian around the period-1 fixed points are outside of the unit circle, hence unstable whereas all the eigenvalues of the period-2 fixed point are inside the unit circle, hence this orbit is stable.

1) Bifurcations: The critical point where a change in stability between the stable period-1 and a stable period-2 orbit occurs is a bifurcation point. One way to show these bifurcations is to take a slice from the stability plot (Fig. 3) while keeping one variable constant. For example, we can fix the amplitude to be $A = 0.8$ while varying the angular frequency ω and plotting one of the state variables, e.g., θ. A bifurcation plot for ω vs. θ is presented in Fig. 4. This

[1]To obtain these nondimensional parameters, this set of parameters can be used: M=0.3 Kg, m=0.7 Kg, L=0.075 m, l=0.06 m, $J_L = 2 \cdot 10^{-5}$ Kgm^2, ω=25 $\frac{\text{rad}}{\text{sec}}$, g=0.98 $\frac{\text{m}}{\text{sec}^2}$, d_{wall}=0.045 m. We note that the set of nondimensional parameters is not unique and could have been chosen differently.

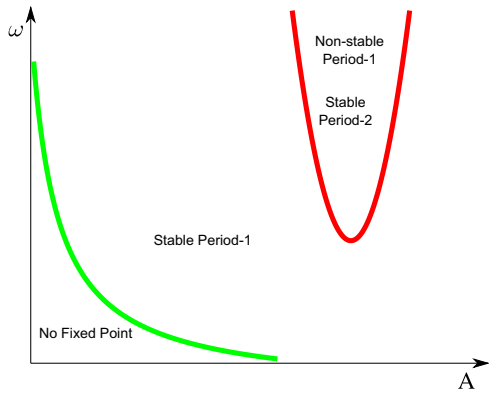

Fig. 3. A-ω stability plot. Three regions of interest are found: bottom left region where no fixed point was found, middle region where a stable period-1 cycles was found, and the top right region where the period-1 turns unstable toghether with a stable period-2 cycle.

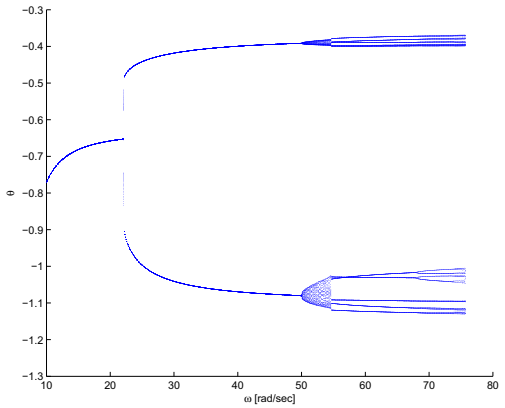

Fig. 4. Bifurcation diagram - leg angle θ vs angular frequency ω. Period-1 in low frequency bifurcates into a period-2 at higher frequencies then into a quasiperiodic and period-10 motion.

bifurcation plot clearly shows the first period doubling at around $\omega \approx 25\frac{\text{rad}}{\text{sec}}$. This is where a period-1 switches to a non-stable orbit while a new, stable period-2 is born. This plot is obtained by forward simulating the Poincaré map a few thousand cycles and plotting the resulting variables. Because this is a forward simulation, we cannot find the unstable (period-1 cycle) as was found in the previous stability plot.

2) Power spectrum analysis: We use the power spectrum analysis tool to further analyze the bifurcation plot (Fig. 4). The power spectrum figures were plotted using Welch's power spectral density method and a Hamming window (see Matlab$^{\text{TM}}$help file). Four input frequencies are investigated (Figs. 5 and 6). In Fig. 5 the period doubling from $\omega = 15\frac{\text{rad}}{\text{sec}}$ to $\omega = 30\frac{\text{rad}}{\text{sec}}$ is evident by noticing that an additional frequency with half of the fundamental one was added to the spectrum. Notice that multiples of the fundamental frequency exists as harmonics. In Fig. 6, we can see two interesting phenomena. In left closeup figure of Fig.6(c), corresponding to $\omega = 55\frac{\text{rad}}{\text{sec}}$, we can see that the points on the Poincaré surface trace a curve, corresponding to quasiperiodic motion. In the right figure, corresponding to

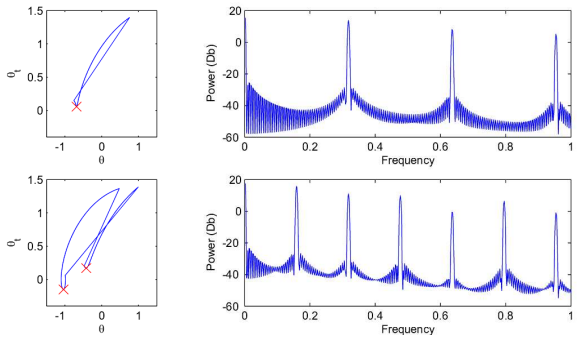

(a) Phase plot (b) Power Spectrum

Fig. 5. Varying ω. 5(a): phase plot (Poincaré points marked with red x), 5(b): power spectrum. Each row represents a different input frequency: $\omega = 15\frac{\text{rad}}{\text{sec}}$, $\omega = 30\frac{\text{rad}}{\text{sec}}$. The change in number of points on the Poincaré plots (marked with X) together with the (nondimensional) frequency in the power spectrum which is half of the fundamental one, reveal a period doubling bifurcation.

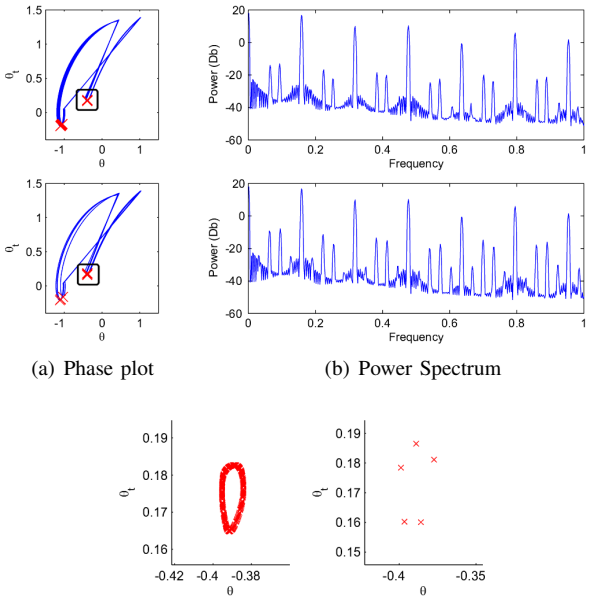

(a) Phase plot (b) Power Spectrum

(c) Poincaré close up

Fig. 6. Varying ω. 6(a): phase plot (Poincaré points marked with red x), 6(b): power spectrum. Top two rows represent different input frequency: $\omega = 55\frac{\text{rad}}{\text{sec}}$, $\omega = 60\frac{\text{rad}}{\text{sec}}$. 6(c) closeups of the Poincaré points (regions marked with square in top rows). The closed curve on the Poincaré map associated with $\omega = 55\frac{\text{rad}}{\text{sec}}$ reveals a quasiperiodic solution while the Poincaré plot of $\omega = 60\frac{\text{rad}}{\text{sec}}$ reveals a period-10 solution (the closeups are on one of the two clusters).

$\omega = 60\frac{\text{rad}}{\text{sec}}$, two regions of five points on the Poincaré section are formed, corresponding to a period-10 motion.

3) Climbing rates: A practical measure of the ability to climb is to measure how far a mechanism climbs during each leap. This corresponds to one Poincaré map. However since asymmetric climbing occurs after the bifurcation points, a better measure might be the average climbing rate, i.e., $\Delta y = \sum_{k=1}^{N} \frac{\Delta y_k}{N}$, where N is the number of maps (approximately 50) and Δy_k is the vertical distance of leap k. Figure 7 shows this average leap for the same parameters as the previous results ($A = 0.8$). A noticeable jump occurs at the bifurcation from period-1 to period-2. Apparently, after

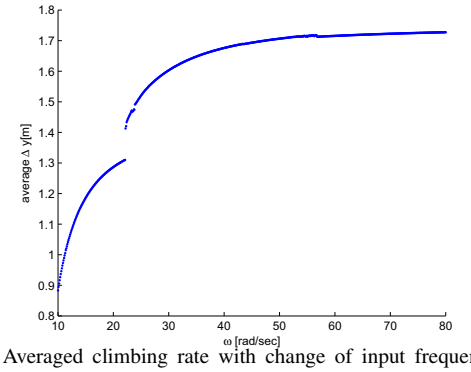

Fig. 7. Averaged climbing rate with change of input frequency (ω). A discontinuous jump in climbing rate occurs at the change from period-1 to period-2.

the period-2 bifurcation, the map initiating at large θ angle climbs significantly more than the period-1 map. Note that period-2 means a leap from one wall with a small θ angle followed by a leap with a large θ angle.

B. Varying mechanism parameters - changing link ratio (l_s)

So far the control inputs (A and ω) have been varied and the stability has been investigated. An important extension to this stability analysis is to examine how the stability changes when mechanism parameters are varied. This section examines how varying the link length ratio changes the local stability.

Figure 8 shows the bifurcation diagram when l_s is varied. This nondimensional parameter, as described earlier, is the link length ratio $l_s = \frac{l}{L}$, corresponding to the ratio between the body length and the leg length. When the link lengths are almost identical ($l_s \approx 1$) corresponding to the right side of Fig. 8, there is a stable period-1 motion. However, when the leg length (L) is elongated, bifurcations start to appear. This is a classic period doubling bifurcation which occurs when one of the eigenvalues exists the unit circle at -1 [11]. One can verify the doubling bifurcations by looking at the power spectral density (PSD) and the points on the Poincaré section as shown in Figure 9. This plot depicts the points on the Poincaré section (9(a)) and the PSD plots (9(b)) for different l_s (with largest on top). These Poincaré section plots show

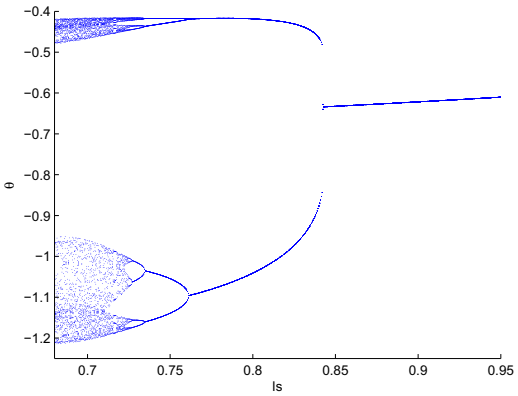

Fig. 8. Bifurcation plot - varying l_s.

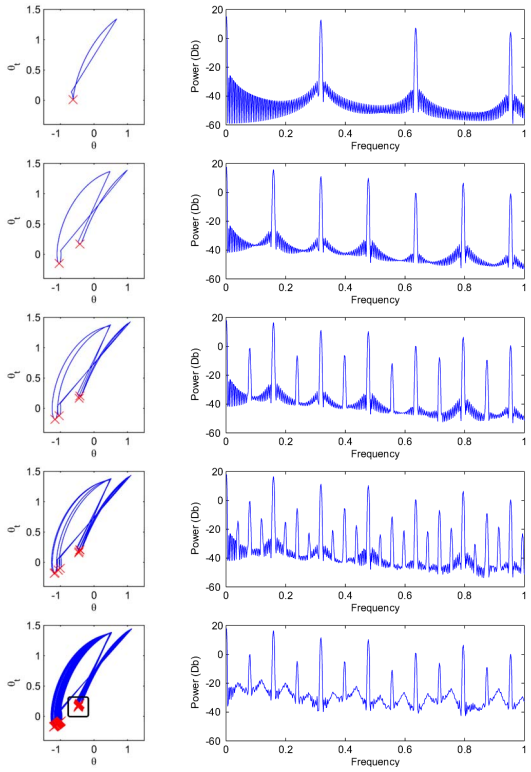

(a) phase plots (b) Power spectrum

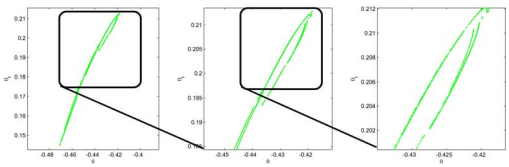

(c) Poincaré plots closeup

Fig. 9. Varying l_s. 9(a): phase plot (Poincaré points marked with red x), 9(b): power spectrum. Each row represents a different leg length ratio (l_s). From top to bottom: l_s=0.9, l_s=0.8, l_s=0.73, l_s=0.715, l_s=0.69. The Poincaré plots and the PSD reveal period doubling bifurcation. 9(c): closeups of Poincaré plots for l_s=0.69 revealing stretching and folding structure characteristic to chaotic-like strange attractor.

the phase plot and crosses marking the point on the section (Poincaré point). For the period-1 motion (top of plot) only the fundamental frequency (and its harmonics) appears on the PSD. Note that the fundamental frequency is normalized to $\pi/10$. On the corresponding Poincaré section only one point appears. On the second plot, an additional frequency appears. This frequency which is half of the fundamental one, corresponds to the first period doubling bifurcation. Once again, on the Poincaré section, two points appear. The bifurcations continue with period-4 and period-8 on the next plots. The bottom plot begins showing evidence of the chaotic region.

VI. EXPERIMENTS

A. Experimental setup

The experimental setup consists of an air table which reduces the out-of-plane motions. The air table also allows us to lower the effective gravity by inclining the table.

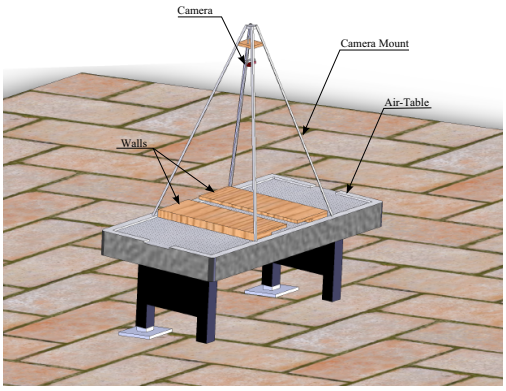

Fig. 10. Air-table and tracking system mounted above.

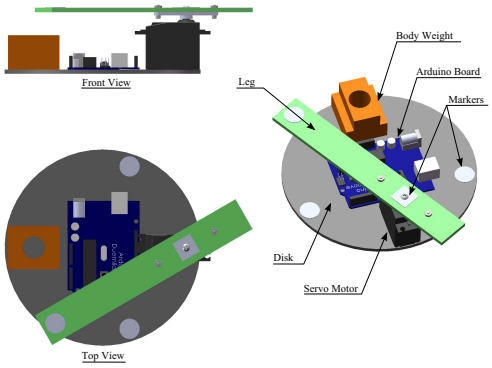

Fig. 11. Current mechanism design.

As discussed earlier, we are using a tenth of the normal gravitational acceleration. In order to record videos of the experiments and track the mechanism, the Optitrack optical tracking system (NaturalPoint^{TM}) is used. This system tracks passive IR markers at rates of 100[Hz]. Since only 2-D motion occur, we use a single camera mounted normal to the surface of the air-table (see Fig. 10).

B. Mechanism design

Our current design (See Fig. 11) consists of a disk which increases the surface area between the mechanism and the air-table. On top of the disk the body mass is connected. On this same disk, a high gear servo motor is connected to a light weight leg. The motor produces the sinusoidal motion of the leg. Two ways can be used to achieve this sinusoidal trajectory: using off board power and controlling it using a PC, or by using an on-board power with a microcontroller.

C. Experimental results

Figure 12 portrays the configuration variables of two climbing motions with different input frequencies. The top, Fig. 12(a), with a sinusoidal angular frequency of $\omega = 15.3\frac{\text{rad}}{\text{sec}}$, and the bottom, Fig. 12(b), with an angular frequency of $\omega = 19\frac{\text{rad}}{\text{sec}}$. These plots are obtained by tracking the markers using the Optitrack system. As was assumed, ϕ is approximately sinusoidal, other than small perturbations during impact. Observing the configuration variable θ, one can see that for the lower frequency (Fig. 12(a)) a symmetric,

period-1 exists. For the higher frequency (Fig. 12(b)) a period-2 appears. On these θ plots, the crosses mark the points on the Poincaré surface including the flip after each impact. This results confirms the period doubling bifurcation as in Fig. 4, section V-A.1. For additional videos of experiments in similar setup see accompanying video or go to `www.dynaclimb.com`.

VII. CONCLUSIONS AND FUTURE WORKS

The mechanism explored in this paper aims to perform stable climbing with minimal design and control complexities. Unique to this mechanism is that it uses dynamic motions to achieve this goal using only a single actuator and a simple symmetric oscillation of the leg. We have shown that by using a well chose Poincaré section we can decrease the dimension of the Poincaré map for analyzing orbital stability to a low, 3-dimensional map. We have explored the orbital stability of this minimalistic mechanism and have shown that for certain continuous parameter changes the symmetric and steady stable gait of the mechanism gradually evolves through a regime of bifurcations.

In future work we intend to generalize the model of this simple 2-link climbing robot, to include more parameters and allow contact with other parts of the robot other than the distal tip of the leg. We intend to perform a wider search over the parameter space, including environment, mechanism, and control parameters, to better understand the system. We further intend to extend the stability analysis to include the basin of attraction (global stability). We will later try and use the information gained in this open-loop analysis and add a simple closed loop to enable climbing in a more complex environment such as piecewise linear walls.

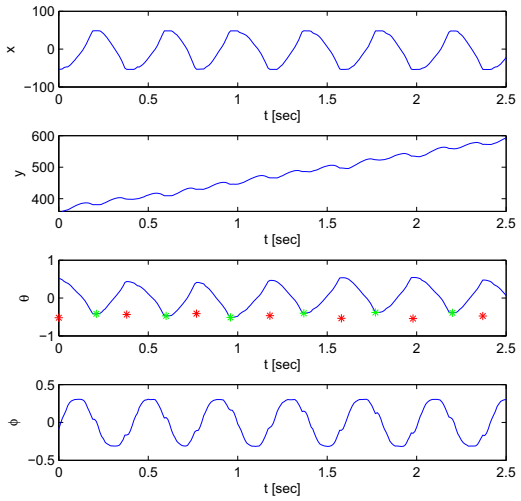

(a) phase plots

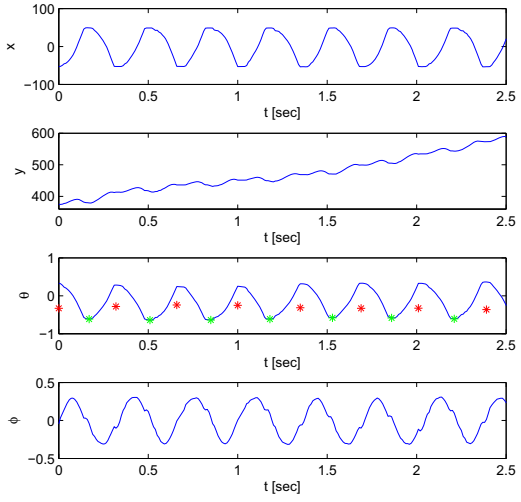

(b) Poincaré plots closeup

Fig. 12. Proof-of-concept experiment – plot of configuration variables. Crosses mark the points on the Poincaré section, including the flip. The plot of the angle ϕ, between to the two links follows the desired sinusoid. The plot of the leg angle θ reveals a symmetric period-1 climbing pattern for $\omega = 15.3 \frac{\text{rad}}{\text{sec}}$ (a), and period-2 for $\omega = 19 \frac{\text{rad}}{\text{sec}}$ (b).

VIII. ACKNOWLEDGMENTS

The authors would like to thank Siyuan Feng, Ben Brown, Kevin Lynch, Andy Ruina, Amir Shapiro, and Oded Gottlieb.

REFERENCES

[1] K. Autumn, M. Buehler, M. Cutkosky, R. Fearing, R. J. Full, D. Goldman, R. Groff, W. Provancher, A. A. Rizzi, U. Saranli, A. Saunders, and D. E. Koditschek. Robotics in scansorial environments. In *Proc. of SPIE Vol. 5804 Unmanned Ground Vehicle Technology VII*, pages 291–302, 2005.

[2] M. D. Berkemeier and R. S. Fearing. Sliding and hopping gaits for the underactuated acrobot. *IEEE Transactions on Robotics and Automation*, 14(4):629–634, August 1998.

[3] T. Bretl. Motion planning of multi-limbed robots subject to equilibrium constraints: The free-climbing robot problem. *The International Journal of Robotics Research*, 25(4):317–342, 2006.

[4] J.F. Canny and K.V. Goldberg. A RISC approach to sensing and manipulation. *Journal of Robotic Systems*, 12(6), 1995.

[5] J. E. Clark, D. I. Goldman, T. S. Chen, R. J. Full, and D. Koditschek. Toward a dynamic climbing robot. In *Proc. of the 9th International Conference on Climbing and Walking Robots (CLAWAR '06)*, Brussels, Belguim, September 2006.

[6] S. H. Collins, M. Wisse, and A. Ruina. A three-dimensional passive-dynamic walking robot with two legs and knees. *International Journal of Robotics Research*, 20(7):607–615, July 2001.

[7] A. Degani. A minimalist dynamic climbing robot: Modeling, analysis and experiments. Thesis Proposal - CMU-RI-TR-09-28, Robotics Institute, Carnegie Mellon Universiy, Pittsburgh, PA, June 2009. `www.ri.cmu.edu/publication_techreports.html`.

[8] A. Degani, A. Shapiro, H. Choset, and M. T. Mason. A dynamic single actuator vertical climbing robot. In *Proc. of IEEE/RSJ International Conference on Intelligent Robots and Systems (IROS'07)*, San Diego, CA, oct 2007.

[9] M. A. Erdmann and M. T. Mason. An exploration of sensorless manipulation. *IEEE Transactions on Robotics and Automation*, 4(4):369–379, August 1988.

[10] M. Garcia, A. Chatterjee, A. Ruina, and M. Coleman. The simplest walking model: stability, complexity, and scaling. *Journal of Biomechanical Engineering*, 120(2):281–288, April 1998.

[11] J. Guckenheimer and P. Holmes. *Nonlinear Oscillations, Dynamical Systems, and Bifurcations of Vector Fields*. Springer, 1983.

[12] D. Longo and G. Muscato. The Alicia^3 climbing robot. *IEEE Robotics and Automation Magazine*, 13:2–10, 2006.

[13] K.M. Lynch and M.T. Mason. Dynamic nonprehensile manipulation: Controllability, planning, and experiments. *International Journal of Robotics Research*, 1999.

[14] T. McGeer. Passive dynamic walking. *The International Journal of Robotics Research*, 9(2):62–82, April 1990.